Hindawi
Advances in Civil Engineering
Volume 2018, Article ID 8410718, 11 pages
https://doi.org/10.1155/2018/8410718

Research Article

Numerical Study of Flame Propagation Morphology for Deflagration in the Pipeline Using Proper Orthogonal Decomposition

Weimin Wu,[1] **Jianyao Yao**,[1,2] **Jingcheng Liu**,[3] **Zejun Wu**,[1] **and Jiawen Liu**[1]

[1]*College of Aerospace Engineering, Chongqing University, Chongqing, China*
[2]*Chongqing Key Laboratory of Heterogeneous Material Mechanics, Chongqing, China*
[3]*Chongqing University of Science and Technology, Chongqing, China*

Correspondence should be addressed to Jianyao Yao; yaojianyao@cqu.edu.cn

Received 27 June 2018; Revised 19 September 2018; Accepted 1 October 2018; Published 29 October 2018

Guest Editor: Guang Xu

Copyright © 2018 Weimin Wu et al. This is an open access article distributed under the Creative Commons Attribution License, which permits unrestricted use, distribution, and reproduction in any medium, provided the original work is properly cited.

A multilevel independent spatial modal analysis of flame propagation characteristics of a deflagration in a specific pipeline was performed using the proper orthogonal decomposition (POD) method, in order to research the evolution process of the explosion which is closely related to flame propagation speed and front rupture pressure. The CFD results indicated that the full-order calculation results well agreed with the normal combustion propagation characteristics of premixed methane-air for the flame propagation with the unbroken thin layer. The POD analysis results showed that the static temperature gradient of the 1st order mode of initial and subsequent stages both exhibited a range of continuity change from left to right, and the frontal curvature of the cooling area decreased as the flame propagated in all stages. The number of the low-temperature interval regions displayed an expanding form of a staircase with the increase of the mode order, especially for subsequent flame in which the interval areas became more and more slender. Moreover, the level of information content in the multilevel modal space was mostly concentrated in the first 3 modes, especially in the 1st order mode, and the flame propagation pattern at the initial stage was more complicated than the subsequent based on the relational information content features.

1. Introduction

The underground mining is the mostly major style of China, in which the wicked environments and geological conditions with complex and varying situation often induce such grave disastrous accidents. The deflagration heads the list of those events, resulting in the destruction of the coal mine ventilation system and the spread of toxic and harmful gases, even inducing that multiple subsurface explosions [1]. The personal security of the staff related and later relief efforts are both dangerously threatened in the complicated circumstances. Therefore, in order to effectively prevent and control these accidents of deflagration, the domestic and overseas scholars have taken many studies about the involved explosion mechanism [2].

Xu et al. [3] investigated the propagation property of deflagration in the roadway with a square cross section of 7.2 m^2 via an experimental test. The results showed that the length of the flame zone was longer than the area of gas accumulation in the explosive evolution and such ratio of differences was up to three to six times. There was a delay interval before the pressure value of monitoring points increased to a maximum value along the propagation path of deflagration. Cheng and Lin [4] studied the influence upon the flame transmission regular pattern in deflagration for tube furcation and pointed out that the additional turbulent flow was produced under the condition of the branch tube, leading to improve the flame transmission speed in the explosion. Lin et al. [5] carried out the experimental research of the influence of barriers for flame transmission and

explosion wave in deflagration. The results indicated that the barriers had a significant impact to the flame transmission and explosion wave, in which the velocity of flame transmission took a sharp increase in the situation with barriers, reaching its maximum value of 20 times L/D ratio. The reason is that the transmission of flame and the turbulent extent of explosive flow can mutually promote each other in the existence of barriers, even resulting in shock wave of explosion to enhance the destructive power in the coal mine tunnels. Li and Gui [6] discussed the flame transmission of deflagration and its acceleration mechanism by experimental and numerical analysis. The results showed that the temperature gradients of front of the flame changed quickly but smoothly in back regions and also manifested that there was a positive feedback for turbulent combustion caused by barriers. Liang and Zeng [7] built a computational model of deflagration to a constant volume bomb through modifying the SENKIN code of CHEMKIN III chemical kinetics package. Using such model, they studied the mole fraction profiles of reactants and the sensitivity of the reaction mechanism of deflagration. The analysis results illustrated that the induced explosion time was prolonged, in which the mole fractions of reactant species such as CH(4) and O(2) and catastrophic gases such as CO, CO(2), and NO were all decreased when water had been added to the mixed gas. Furthermore, the sensitivities of reactions to species of CH(4) and CO(2) were also depressed with the water fraction increasing. Lukashov [8] proposed the sequential use of two mathematical models to compute the deflagration of a coal mine. One of the models was applied to obtain the propagation of air shock waves and another for the computation of the air distribution in the mine situation. The given approach can more precisely estimate the situation of explosion in the mine and identify the regions affected by shock waves and the distributed explosion products. Nie et al. [9] conducted the experimental study of a rectangular explosion test pipe to substantially suppress the shock waves of deflagration for coal mines. The results demonstrated that the foam ceramics can buffer the explosion overpressure by up to fifty percent and the interconnected micronetwork structure of the foam ceramics can help us to quench the flame of explosion. Yu et al. [10] experimentally investigated the effects of the hollow-square obstacle in deflagration by constructing a semiconfined transparent chamber. The research showed that the triangular hollow-square obstacle caused the highest turbulent intensity, flame propagating velocity, and overpressure, whereas the lowest values were for the circular hollow square. Pei et al. [11] discussed the synergistic inhibition effect of nitrogen and ultrafine water mist for deflagration in a ventilated pipe. The experimental data displayed that propagation speed and overpressure of the peak flame declined significantly with the increase of fraction of nitrogen and spraying time of water. However, the explosion inhibition efficiency was gradually decreased as the continuous increase for water mist and nitrogen. Liu and Jia [12] established the overpressure prediction model for deflagration shock wave using the theory of explosion similarity, and the model was well verified by means of relevantly experimental data. Other domestic and international research progress can be found in the literatures [13–17].

Although scholars have carried out a variety of studies for deflagration, the traditionally experimental and numerical analysis are still limited for the further investigation of the mechanism of deflagration. In the research of the deflagration mechanism, the flame propagation pattern is a very important feature, which can greatly affect the speed of flame propagation and the membrane rupture pressure to flame front. Therefore, it is necessary to employ more advanced method to study such morphological changes of explosion flame. In this paper, the proper orthogonal decomposition (POD) method is used to research the evolution process of combustion explosion propagation in a pipeline. The paper has five more sections. The basic theories of deflagration and POD method are introduced in Sections 2 and 3. And the CFD model and the data interface program are developed in Section 4. The numerical results are discussed in Section 5, and some conclusions are drawn in the last section.

2. Physical and Mathematical Models for Deflagration in a Pipeline

It is an essential part to the analysis of deflagration in the underground passage of a mine, which includes the physical model and the description of mathematics, respectively.

2.1. Physical Model. In the light of such deflagration theory [18], there are two courses of the burning explosion in a pipeline, including the initial ignition stage of hot products and subsequent propagation stage for premixed reactants for coal mine gas in the underground operation channel. The essential process of an entire explosion can be understood as the propagation of combustion and shock waves from ignition and burning new premixed gas areas to the regions of unburned-premixed areas. The physical model of deflagration in the pipeline is shown simplistically in Figure 1.

It is worth noting that the deflagration process is in an ideal condition without obstacles in the coal mine passage. For more complicated situations, one can refer to the literatures [19, 20].

2.2. Mathematical Model. The deflagration inside the pipeline is a rapid reaction process of combustion, in which the related equations of control should be satisfied, including the mass conservation equation, momentum conservation equation, energy conservation equation, and the chemical composition equilibrium equation. The description of turbulence follows the standard $k-\varepsilon$ model, which is shown in the following equations:

$$\frac{\partial}{\partial}(\rho k)+\frac{\partial}{\partial x_i}(\rho k u_i)=\frac{\partial}{\partial x_j}\left[\left(\mu+\frac{\mu_t}{\sigma_k}\right)\frac{\partial k}{\partial x_j}\right]+G_k+G_b-\rho\varepsilon - Y_M+S_k, \tag{1}$$

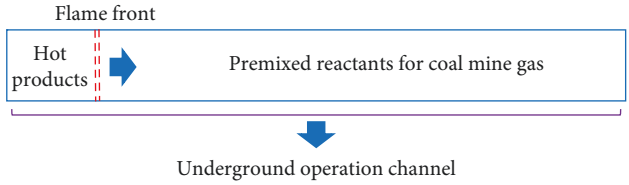

Figure 1: Physical model of deflagration process in the pipeline.

and

$$\frac{\partial}{\partial t}(\rho\varepsilon) + \frac{\partial}{\partial x_i}(\rho\varepsilon u_i) = \frac{\partial}{\partial x_j}\left[\left(\mu + \frac{\mu_t}{\sigma_\varepsilon}\right)\frac{\partial \varepsilon}{\partial x_j}\right] + C_{1\varepsilon}\frac{\varepsilon}{k}\left(G_k + C_{3\varepsilon}G_b\right) - C_{2\varepsilon}\rho\frac{\varepsilon^2}{k} + S_\varepsilon. \tag{2}$$

According to the above transport equations, the turbulence kinetic energy, k, and its rate of dissipation, ε, can be obtained, respectively. G_k represents the generation of turbulence kinetic energy due to the mean velocity gradients, and G_b is the generation of turbulence kinetic energy due to buoyancy. Y_M represents the contribution of the fluctuating dilatation in compressible turbulence to the overall dissipation rate. Those $C_{1\varepsilon}$, $C_{2\varepsilon}$, and $C_{3\varepsilon}$ are constants. σ_k and σ_ε are the turbulent Prandtl numbers for k and ε.

The turbulent viscosity, μ_t, is computed by combining the turbulence kinetic energy and dissipation rate [21], in which the values of the model constants have been determined from experiments for fundamental turbulent flows including frequently encountered shear flows like boundary layers, mixing layers, and jets as well as for decaying isotropic grid turbulence.

The conservation equations for chemical species takes the following general form, which predicts the local mass fraction of each species, Y_i, through the solution of a convection-diffusion equation for the species:

$$\frac{\partial}{\partial t}(\rho Y_i) + \nabla\cdot\left(\rho\vec{v}Y_i\right) = -\nabla\cdot\vec{J}_i + R_i + S_i, \tag{3}$$

where R_i is the net rate of production of species i by chemical reaction and S_i is the rate of creation by addition from the dispersed phase plus any defined sources. $\vec{J}_i$ is the diffusion flux of species i, which arises due to gradients of concentration and temperature [22].

3. Proper Orthogonal Decomposition for Deflagration

The POD method can quantitatively analyze the essential information of the flow at multiple levels so that the main features of the flow can be more accurately captured for further analysis. The method is generally divided into continuous type and discrete type. However, the discrete POD method is more commonly used because of the difficulty in obtaining the analytical basis function in practical research. Therefore, only the discrete POD method is introduced here, combining deflagration parameters in a pipeline.

3.1. Discrete-Type Proper Orthogonal Decomposition. The deflagration parameter values of a series of discrete points, obtained by the full-order numerical method under the same transient moment conditions, are arranged in a specific order to obtain the required sample vector $g(\mathbf{x}, t_m)$. The corresponding form is as follows:

$$g(\mathbf{x}, t_m) = \left[\, g(x_1, t_m)\ \ g(x_2, t_m)\ \cdots\ g(x_n, t_m)\ \cdots\ g(x_N, t_m)\,\right]^T, \tag{4}$$

where N is the total number of discrete points in such a physical model.

The sample matrix $\mathbf{G}$ can be formed by arranging the sample vectors in the sequence of time evolution, in which the size of this sample matrix is worthy for further discussion, especially for the time dimension:

$$\mathbf{G} = \left[\, g(\mathbf{x}, t_1)\ \ g(\mathbf{x}, t_2)\ \cdots\ g(\mathbf{x}, t_m)\ \cdots\ g(\mathbf{x}, t_M)\,\right], \tag{5}$$

where M is the total number of sample vectors, also named the total number of snapshots in a large number of related studies.

Under the same number of snapshots, mathematical transformations and decompositions are needed in order to find the best orthogonal basis functions in discrete form. Therefore, the covariance matrix should be calculated first [23]:

$$\mathbf{C} = \mathbf{G}^T\mathbf{G}. \tag{6}$$

It is worth noting that such $\mathbf{C}$ is a real symmetric matrix and has nonnegative eigenvalues. Therefore, the problem of finding the optimal orthogonal basis function is transformed into the solution of the following eigenvalues:

$$\mathbf{C}\mathbf{H}^{[r]} = \lambda_r\mathbf{H}^{[r]}, \tag{7}$$

where $\mathbf{H}^{[r]}$ is the rth eigenvector for the deflagration parameter, and the quantity λ_r is the eigenvalue corresponding to the rth-order POD mode of explosion flow parameter:

$$\mathbf{H}^{[r]} = \left[\, h^r(t_1)\ \ h^r(t_2)\ \cdots\ h^r(t_m)\ \cdots\ h^r(t_M)\,\right]^T. \tag{8}$$

The rth-order POD mode of the explosion flow field can be defined by

$$g_r(\mathbf{x}) = \frac{1}{M\lambda_r}\sum_{m=1}^{M} h^{[r]}(t_m)\, g(\mathbf{x}, t_m), \tag{9}$$

where such eigenvalue corresponding to each eigenvector is sorted in decreasing order for the information content contribution to the explosion flow field. Therefore, the major flow characteristics of deflagrations can be extracted using low-order POD flow modes, in order to analyze the most important flow essential information.

3.2. Definition of Information Contribution for Deflagration in a Pipeline. The quantitative analysis of the multilevel flow features of the POD method is mainly reflected in the feature value level corresponding to the feature projection direction.

The global average information content to explosion flow may be described as

$$E = \frac{1}{2}\sum_{r=1}^{M}\lambda_r = \sum_{r=1}^{M}E_r, \tag{10}$$

where E is the global average pulsating information content for a burning explosion flow field, E_r is the information content of one specified such flow mode, and λ_r is the eigenvalue of the corresponding spatial mode.

In the light of Equation (10), there are two quantitative indicators of the information content of the explosion flow mode, defined as follows:

$$\eta_r = \frac{\lambda_r}{\sum_{m=1}^{M}\lambda_m}, \qquad \kappa_r = \frac{\sum_{m=1}^{r}\lambda_m}{\sum_{m=1}^{M}\lambda_m}, \tag{11}$$

where η_r refers to the single-order contribution of information content for the rth order mode and κ_r represents the cumulative contribution of information content for the modes up to order r. That quantities η_r and κ_r are representative of quantitative indicators obtained upon averaging the pulsating energy contribution for the velocity-type parameters in the physical field.

In this investigation, such propagation characteristics of deflagration in the designated barrier-free pipeline were studied, making use of the discrete-type POD method based on the results of full-order numerical calculation. Therefore, it is necessary to introduce the corresponding CFD model for the explosion flow.

4. CFD Model for Deflagration in the Pipeline

In order to improve the efficiency of full-order numerical computations, the two-dimensional flow area was adopted, combined with a layout strategy of the isotropic structured grid. The length of the pipe model is 18 m, and the width is 0.2 m. The rectangular channels were 9.5 percent methane-air premixed gas filled, ignoring the pipe thickness.

4.1. Grid Layout for the Pipeline. There are 30 points in the width direction and 2700 points in the length direction, which is a total number of 81000 with quadrilateral elements in such domain. The CFD model is shown in Figure 2.

4.2. Initial and Boundary Conditions. For the CFD model of uniform premixed deflagration, the four boundaries of the numerical calculation area are all set to the adiabatic wall, with room temperature 300 K. The relative roughness of the walls are all set to 0.05 mm and the related roughness height in such rough wall formulation is set to 0.02, taking into account the actual coal mining channel situation. In addition, the heat flux per unit area of the wall is set to 0, and the species boundary condition for CH(4), O(2), CO(2), CO, and H(2)O are designated as zero diffusive flux type.

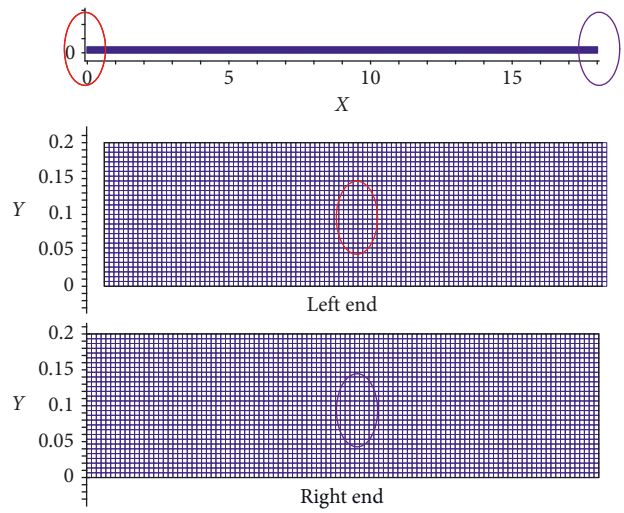

Figure 2: Grid layout of deflagration for the pipeline.

The initial gas mixture state included the temperature of 300 K, the pressure of a standard atmosphere, and both velocities specified to be zero along X and Y directions. When methane-air premixed gas concentration is 9.5 percent, the mass fraction of each component was 5.3 percent of CH(4), 21 percent of O(2), 73.7 percent of N(2), and both 0 percent of H(2)O and CO(2), respectively. For the stability and reliability of subsequent calculations, the computation of 50 time steps under this condition was performed and checked.

Then, the model needs to set ignition initial conditions for deflagration. According to the thermal ignition theory, the region of high-temperature gas can be set as the ignition zone during the explosion simulation. Here, the left end of the pipeline was set to the ignition position, and the temperature of the local area and the mass fraction of each component at the beginning of the ignition were the temperature of 1400 K, both 0 percent of CH(4) and O(2), 73.7 percent of N(2), 14.5 percent of CO(2), and 11.8 percent of H(2)O, respectively.

It is worth noting that, in order to be closer to the actual situation, the initial ignition area is set to a smaller semicircular area. Its center coordinates are (0, 0.1) with radius 0.02 m, which corresponds to the center of the left end of the channel.

4.3. Interface Program to Realize POD-CFD Analysis. In order to achieve POD multilevel analysis of flame propagation patterns of deflagration in the pipeline, an interface program for the POD-CFD calculation of the specified field variable was developed to enable subsequent analysis using full-order CFD numerical calculation results. The logical framework of the interface program is shown in Figure 3.

The interface program consists of three parts. (1) It is data structure conversion which is for binary output files generated by high-confidence CFD code. (2) In this step, the secondary conversion of the basic data for POD analysis is realized by the in-house Matlab code. Among them, the homology processing corresponding to the data structure is

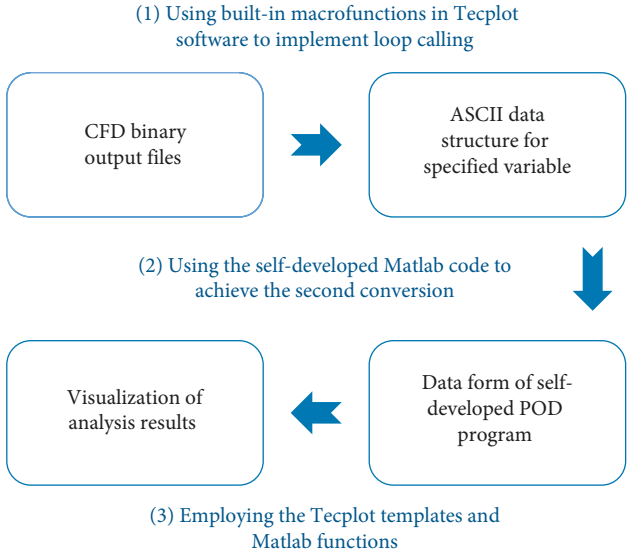

Figure 3: Interface program of data structure for the POD-CFD calculation.

included. (3) Tecplot template and related Matlab functions were used to visualize the POD analysis results. Among them, for the built-in related macrofunctions, the corresponding subroutine for loop calling is developed.

5. Analysis of Numerical Results

5.1. Full-Order Computational Results for Pipeline Explosion. According to the condition settings of definite solution of deflagration, combining such methane combustion reaction equations, the results were manifested at the different characteristic moments for the main reaction phase upon the flame propagation in Figure 4.

In the light of Figure 4, the development trend of the initial static temperature field and the subsequent propagation of the flame are coherently presented based on advancement of deflagration time. The average speed of flame propagation for the unbroken thin layer is approximately 0.47 m/s, which meets the normal combustion propagation characteristics of premixed methane-air. In order to more clearly characterize the flame propagation process in the early stage of an explosion, the following analysis is performed in conjunction with Figure 5.

According to the flame propagation pattern of Figure 4, the average flame propagation velocity between the adjacent monitoring moments can be calculated. The corresponding situation is shown in Figure 5. Due to the energy excitation that initiates the ignition, the average flame propagation velocity at the relevant initial stage is faster. In the later stage of stable flame propagation, the corresponding average axial propagation velocity is kept within 0.5 m/s.

In Figure 6, the nonblue area on the left indicates that the gas has started to burn rapidly and the maximum static temperature has reached more than 2400 K. The blue area on the right indicates that the original premixed gas has not yet started to burn and is only affected by the disturbance of the left-side explosion combustion shock wave, and the temperature is relatively low.

Moreover, after the left-hand premixed gas is ignited, the static temperature rises rapidly and forms a spherical flame. Over time and with the special setting of the above ignition zone, the combustion flame gradually appears hemispherical to the right in the pipeline, which specifically corresponds to the time points of 1, 2, and 3. At the same time, considering the constraints of the upper and lower walls of the pipe itself and the reflection effect, the axial velocity of flame propagation is much greater than the radial velocity. Due to the difference of the axial and radial propagation speeds, the combustion flame gradually stretches and lengthens in the axial direction and turns into an ellipsoidal shape. As the flame propagates, the curvature of the flame front and the highest local static temperature both decrease in the pipeline, obviously corresponding to time points 4 to 7.

For subsequent flame propagation characteristics, shown in Figure 4, the local maximum static temperature regions corresponding to time points 8, 9, and 10 are further reduced during the flame spread. In order to intuitively reflect the changing characteristics of subsequent flame propagation speeds, the time points of equal time intervals were used, from 11 to 25. Due to the impacts of the combustion shock wave and wall surface, it clearly shows that, as the flame continues to propagate backwards in the pipeline, its speed of propagation continues to decrease, and the curvature of the flame front is still decreasing in Figure 7, especially for the time points 23 and 25. In addition, the change regions of the high static temperature gradient are also concentrated near the thin layer of the flame front for the different follow-up moments of combustion.

5.2. POD Analysis for Computational Results. In order to understand deeply the morphological characteristics of the flame propagation for deflagration in the pipeline, the POD method is used here, specifically for the initial stage of explosive combustion and typical subsequent propagation stages.

For the initial stage of POD analysis, the start time of the sample data is the time corresponding to the time point 1 in Figure 4, that is, the time of the explosion combustion at 0.001 s. Then, taking 0.001 s as the equal time interval, a total of 600 full-order numerical transient solutions were selected in the order of the evolution of the explosion time to form the sample matrix for the initial phase analysis.

For the analysis of such stably subsequent propagation of flame, the initial time is selected as the 13 time point shown in Figure 4, the time interval is still set to 0.001 s and the same total of 600 full-order transient solutions. The sample matrix is in the same form as the initial stage. Because the follow-up flame propagation patterns of deflagration have high similarity with each other, no other subsequent stages are selected for POD correlation analysis here.

The dimensionless flame propagation modes in the pipeline in the initial stage for the first 9 orders are manifested in Figure 8, and the subsequent first 9 orders dimensionless modes are shown in Figure 9.

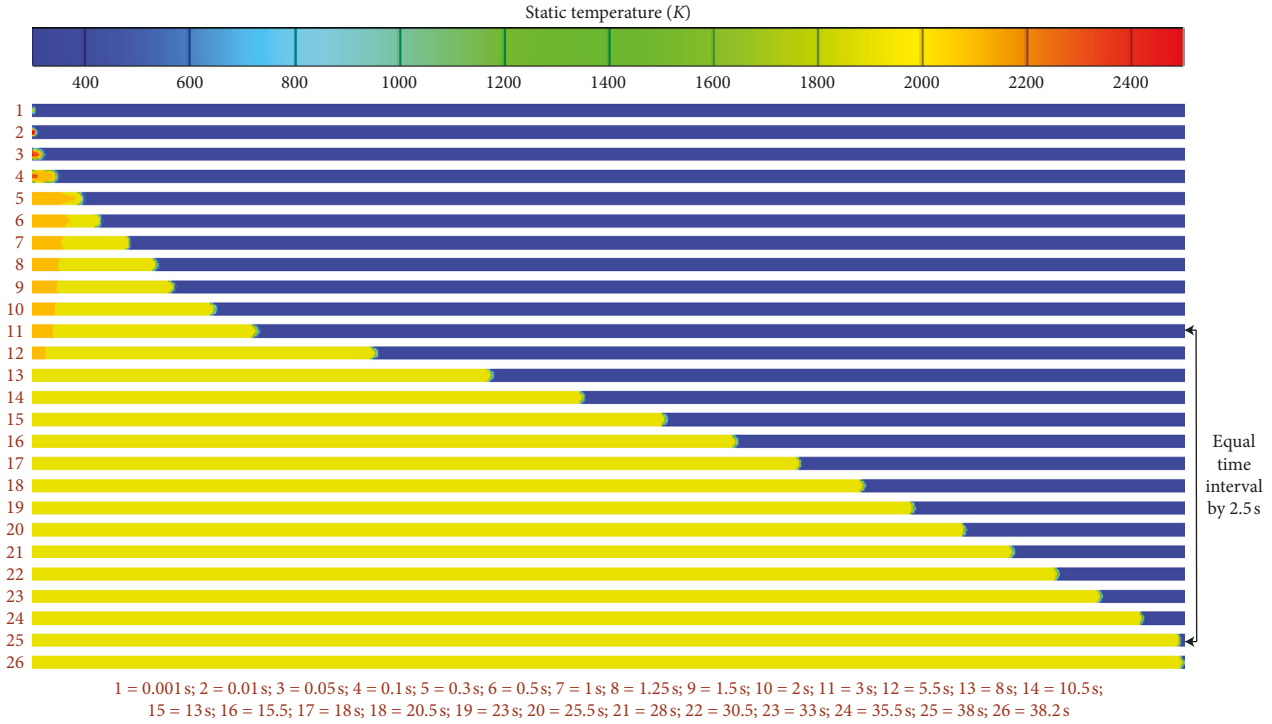

Figure 4: Flame propagation process of deflagration upon static temperature in the pipeline.

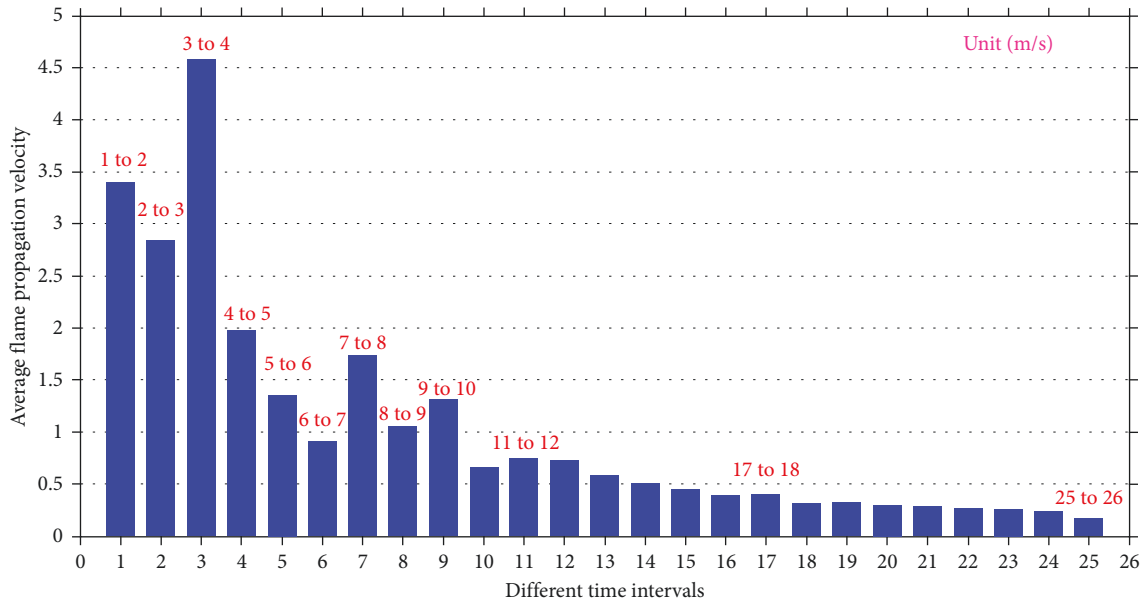

Figure 5: Flame propagation velocity of deflagration in the pipeline.

According to Figure 8, the static temperature gradient of the 1st-order mode of initial stage exhibits a wide range of continuity changes from left to right, and the cooling gradient intensifies as the rightward propagation distance increases. Furthermore, as the flame propagates backward, the frontal curvature of the cooling area decreases. The 2nd and 3rd modes both begin to show a low-temperature interval area in the right direction of the pipeline, and the left parts of such 2nd and 3rd modes exhibit the characteristics of opposite changes with orthogonality. From the 4th mode, the increase in the number of static temperature variation interval area in the pipeline occurs. With the increase of the mode order, the number of the interval regions shows an expanding in the form of a staircase, in which the 4th and 5th modes are 2 low-temperature interval regions, and the 6th and 7th orders are 3 such interval regions, as well as the 8th and 9th orders are 4 low-temperature interval regions. It is obvious that the ranges of the low-temperature interval and

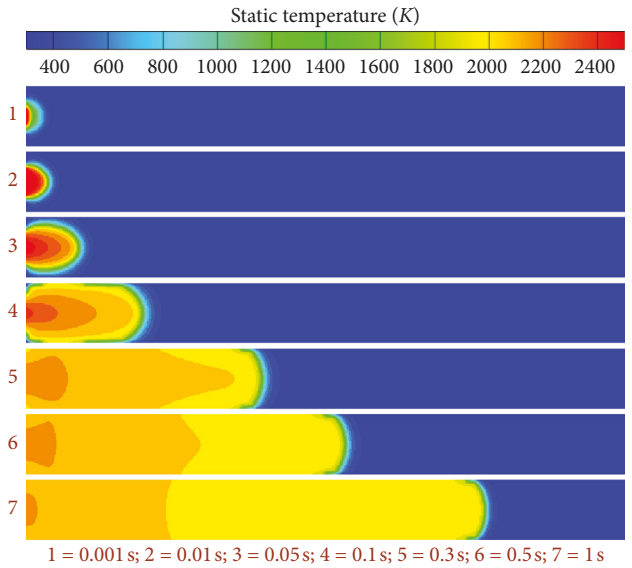

Figure 6: Flame propagation characteristics of deflagration at the initial stage.

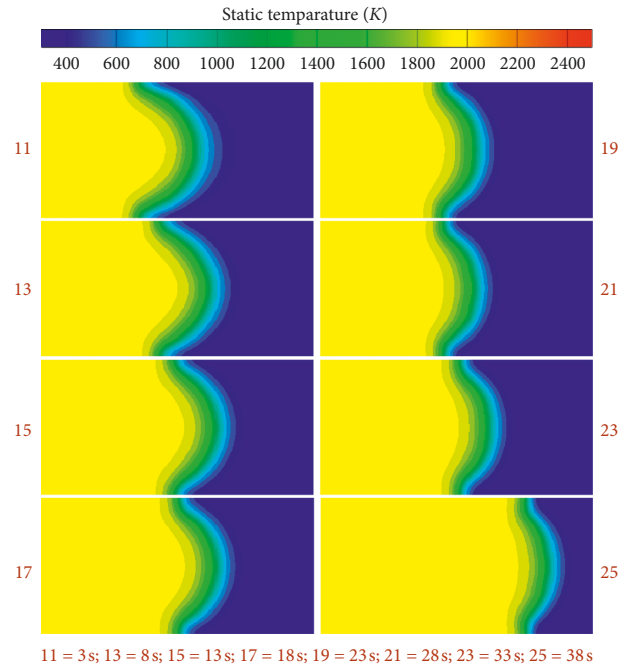

Figure 7: Flame propagation characteristics of deflagration in the subsequent stages.

cooling areas gradually decrease from the 4th to the 9th order. The right-most static temperature change regions of the 4th and 5th orders are represented by orthogonality correspondence, while the 6th, 7th, and 8th and 9th orders have similar characteristics.

According to Figure 9, the subsequent flame propagation frontal morphology can be decomposed into multiple levels of independent spatial existence. The 1st-order mode still shows continuous gradient cooling characteristics; however, because the subsequent flame propagation front has a smaller impact range than the initial stage of combustion,

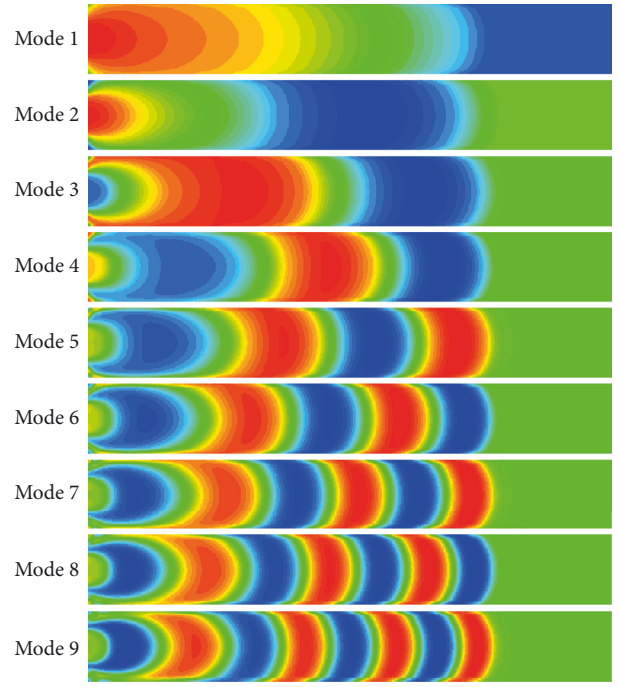

Figure 8: Flame propagation of the initial stage for the dimensionless at the first 9 different modes.

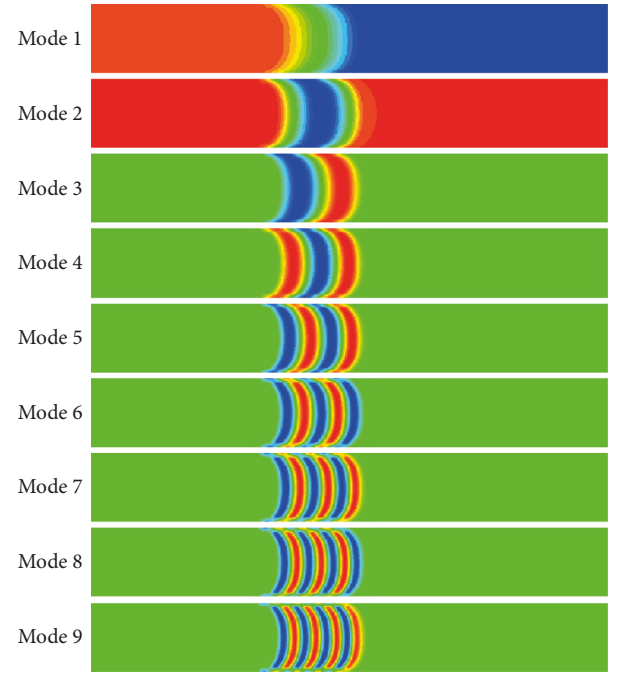

Figure 9: Flame propagation of the subsequent stage for the dimensionless at the first 9 different modes.

the 1st-order mode static temperature variation range is also smaller than the initial stage of the same order mode.

The 2nd-order mode has a low-temperature interval region, and it displays the orthogonality of the region corresponding to the right part of the 1st-order mode. The 3rd-order mode has a high-temperature cooling region after the low-temperature interval area. It is very interesting that

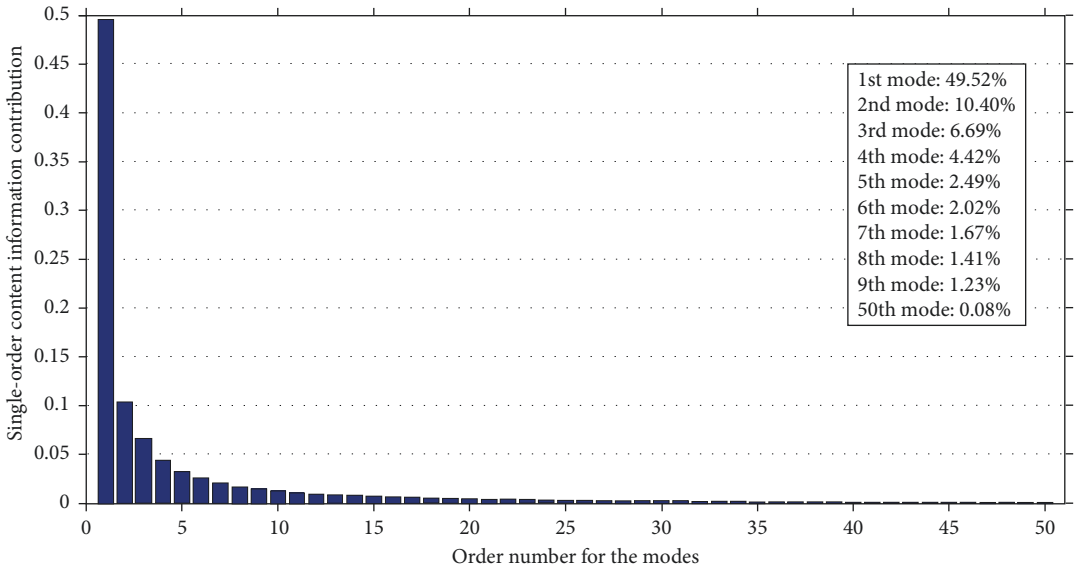

Figure 10: Single-order content information contribution for the first 50 modes in the initial stage of flame propagation.

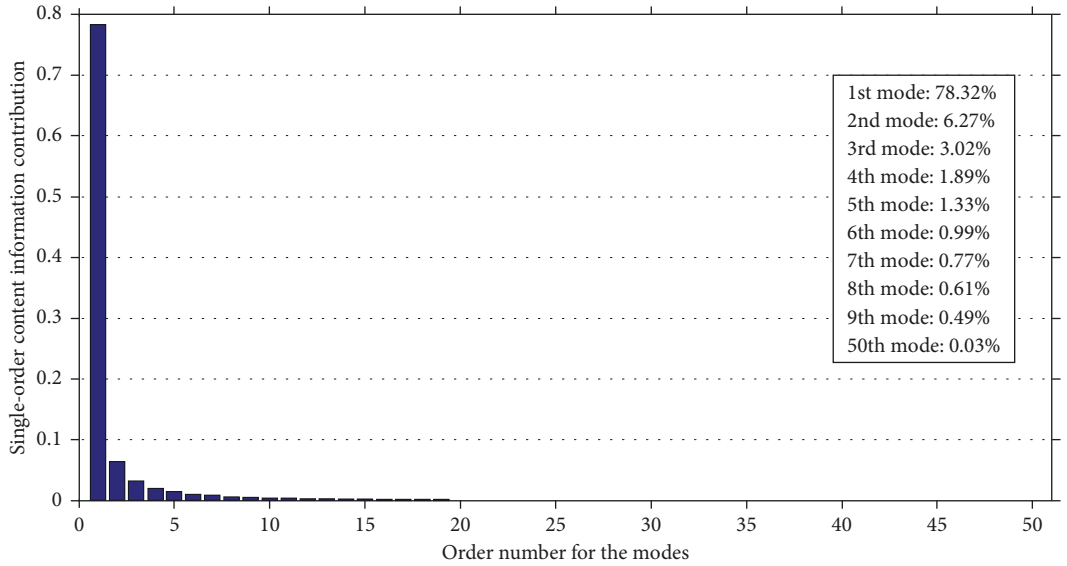

Figure 11: Single-order content information contribution for the first 50 modes in the subsequent stage of flame propagation.

the total number of low-temperature interval and high-temperature cooling regions increases linearly as the mode order heightens from the 3rd to the 9th order. The further observations found that such 2 kinds of interval areas become more and more slender with the increase of the mode order.

To further analyze the quantitative effect of these multilevel independent spatial modalities on the overall flame propagation morphological characteristics, according to such formula (11), the single-order content information contribution level of initial explosion and subsequent combustion propagation stages were both obtained, shown separately in Figures 10 and 11.

In the light of Figure 10, the influence of the 1st-order mode information ratio in the initial combustion stage is almost 50 percentage; therefore, it has the greatest impact on the overall flame propagation pattern. The 2nd-order to the 9th-order modes also have an important influence on the integral flame propagation shape, in which the smallest modal effect ratio of 9th order has exceeded 1.2 percentage; especially for the 2nd and 3rd modes, they approximately reached 10.4 and 6.69 percentages, respectively. The influence of such 50th-order is relatively negligible, only about 0.08 percentage.

Then, with the analysis of Figure 11, the multilevel spatial modal information in the subsequent propagation stage is generally consistent with the distribution of the influence characteristics in the initial stage. However, the proportion of the 1st-order modal information exceeds 78.3 percentage, which is obviously higher than the influence of the same order proportion in the initial stage. Moreover, the levels of the 2nd-order to the 9th-order modal information content all are

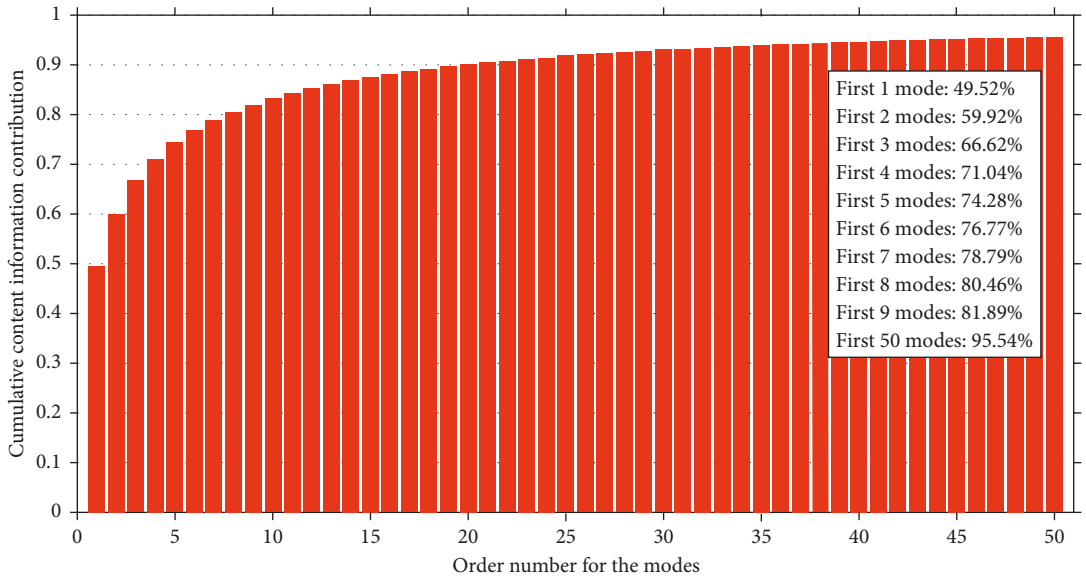

Figure 12: Cumulative content information contribution for the first 50 modes in the initial stage of flame propagation.

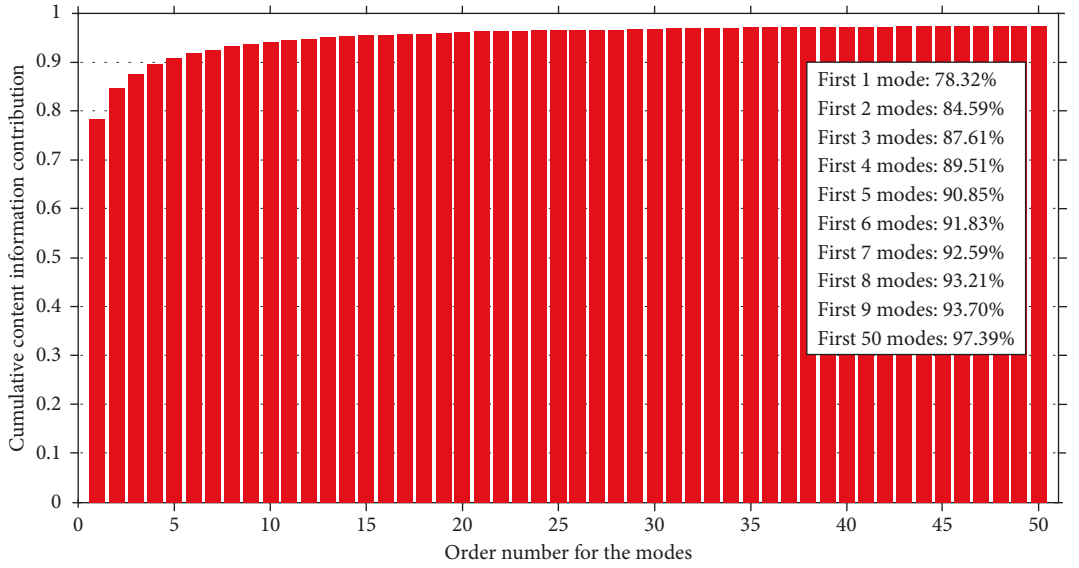

Figure 13: Cumulative content information contribution for the first 50 modes in the subsequent stage of flame propagation.

lower than the same order modes of the initial stage, respectively. For the 50th-order mode, the information content is also significantly lower than the initial explosion stage.

The modal cumulative content information contribution characteristics of the initial explosion stage and subsequent propagation stage are shown in Figures 12 and 13, respectively. For the first 9 modes, the latter 93.7 percentage is significantly higher than the former 81.89 percentage. To the first 50 modes, the latter 97.39 percentage is still higher than the former 95.54 percentage.

Based on the above information content analysis, the level of information content in the multilevel modal space of deflagration is mostly concentrated in the first 3 modes, especially for the 1st-order mode. Moreover, the modal information content concentration level of such subsequent propagation stage is higher than the initial explosion stage. Therefore, it shows that the flame propagation pattern at the initial explosion stage is more complicated than the subsequent stage, and for more detailed research, the initial stage needs to involve more high-information content modalities, not only the first 9 modes.

6. Conclusions

A multilevel independent spatial modal analysis of the flame propagation characteristics of a deflagration in a specific pipeline was performed, using such proper orthogonal decomposition method. In order to implement the POD-CFD deflagration analysis, an interface program was developed, which can realize the conversion from the CFD binary

output files to the POD calculation basic data structure and also includes those visualizations of numerical results.

The full-order numerical calculation results manifested that the local maximum static temperature exceeded 2400 K in the initial stage of the explosion combustion, and the combustion flame gradually stretched and lengthened in the axial direction and turns into an ellipsoidal shape because of the difference of the axial and radial propagation speeds in the pipeline. Moreover, the curvature of the flame front and the highest local static temperature both decreased as the flame propagated. For subsequent flame propagation characteristics, the local maximum static temperature regions were further reduced and the corresponding speed of propagation and the curvature of the flame front continued to decrease, especially for the late stage of combustion. In general, the full-order calculation results well agreed with the normal combustion propagation characteristics of premixed methane-air for the flame propagation with the unbroken thin layer. Therefore, the above numerical calculation results are reasonable and effective.

The POD analysis results showed that the static temperature gradient of the 1st-order mode of the initial stage exhibited a wide range of continuity changes from left to right and the frontal curvature of the cooling area decreased as the flame propagated backward. The higher modes all showed the low-temperature interval area in the right direction of the pipeline and some of them with opposite changes in orthogonality. The number of the low-temperature interval regions displayed an expanding in the form of a staircase with the increase of the mode order. For the subsequent flame propagation frontal morphology, the 1st-order mode still showed continuous gradient cooling characteristics; however, the 1st-order mode static temperature variation range is smaller than the initial stage of the same order mode. The further observations found that the interval areas became more and more slender with the increase of the mode order. According to the modal information content analysis, the level of information content in the multilevel modal space of deflagration is mostly concentrated in the first 3 modes, especially for the 1st-order mode, and the flame propagation pattern at the initial explosion stage is more complicated than the subsequent stage.

Furthermore, this type of interface program is also suitable for POD analysis of deflagration in pipelines with obstacles, which is a next plan for further analysis of deflagration. Due to the influence of the obstacle on the fine structure of the deflagration flame in the pipeline, it will cause secondary deflagration with the coal dust cloud and strengthen the turbulence of the internal flow field of the flame, thereby accelerating the propagation of the flame in the pipeline. Therefore, it is necessary to make a deeper analysis of the relevant situation. In the subsequent analysis, the interface program with practical value of engineering analysis will also be further developed.

Data Availability

All the basic data in the article are available, including in-house interface program.

Conflicts of Interest

The authors declare that they have no conflicts of interest.

Acknowledgments

This work is funded by the National Natural Science Foundation of China (No. 11502037), the Chongqing Research Program of Basic Research and Frontier Technology (No. cstc2018jcyjA3066), and the Fundamental Research Funds for the Central Universities (No. 2018CDGFHK0019).

References

[1] D. Bjerketvedt, J. R. Bakke, and K. V. Wingerden, "Gas explosion handbook," *Journal of Hazardous Materials*, vol. 52, no. 1, pp. 1–150, 1997.

[2] R. Dobashi, "Experimental study on gas explosion behavior in enclosure," *Journal of Loss Prevention in the Process Industries*, vol. 10, no. 2, pp. 83–89, 1997.

[3] J. Xu, S. Xu, and G. Yang, "Experiment study on mine gas explosion transmission," *Coal Science and Technology*, vol. 32, no. 7, pp. 55–57, 2004.

[4] Z. Cheng and B. Lin, *Experimental Research of Tube Furcation's Influence on Flame Transmission Speed in Gas Explosion*, Jiangsu Coal, Jiangsu, China, 2004.

[5] B. Lin, S. Zhou, and R. Zhang, "Influence of barriers on flame transmission and explosion wave in gas explosion," *Journal of China University of Mining and Technology*, vol. 28, no. 2, pp. 53–57, 1999.

[6] B. Q. Li and X. H. Gui, "Numerical simulation research on flame transmission in gas explosion," *Journal of China University of Mining & Technology*, vol. 31, no. 1, pp. 29–32, 2002.

[7] Y. Liang and W. Zeng, "Numerical study of the effect of water addition on gas explosion," *Journal of Hazardous Materials*, vol. 174, no. 1–3, pp. 386–392, 2010.

[8] O. Y. Lukashov, "On an integrated approach to modeling an emergency under a gas explosion in a coal mine," *Institute of Coal of the Siberian Branch of the RAS*, vol. 19, no. 6, pp. 86–93, 2014.

[9] B. Nie, X. He, R. Zhang, W. Chen, and J. Zhang, "The roles of foam ceramics in suppression of gas explosion overpressure and quenching of flame propagation," *Journal of Hazardous Materials*, vol. 192, no. 2, pp. 741–747, 2011.

[10] M. Yu, K. Zheng, and T. Chu, "Gas explosion flame propagation over various hollow-square obstacles," *Journal of Natural Gas Science and Engineering*, vol. 30, pp. 221–227, 2016.

[11] B. Pei, M. Yu, L. Chen, X. Zhu, and Y. Yang, "Experimental study on the synergistic inhibition effect of nitrogen and ultrafine water mist on gas explosion in a vented duct," *Journal of Loss Prevention in the Process Industries*, vol. 40, pp. 546–553, 2016.

[12] T. Liu and J. Jia, *Overpressure Prediction of Gas Explosion Shock Wave in Excavation Roadway of Coal Mine*, Mining Safety & Environmental Protection, vol. 44, no. 5, pp. 18–20, 2017.

[13] V. S. Babkin and P. K. Senachin, "Classification of similarity criteria in combustion theory and the problem of autoignition of a combustible mixture by compression," *Combustion, Explosion, and Shock Waves*, vol. 54, no. 3, pp. 275–283, 2018.

[14] V. A. Strunin and L. I. Nikolaeva, "Combustion mechanism of RDX and HMX and possibilities of controlling the;

combustion characteristics of systems based on them," *Combustion, Explosion, and Shock Waves*, vol. 49, no. 1, pp. 53–63, 2013.

[15] Y. Zhang, D. U. Wenzhou, Y. Wang et al., *Combustion and Explosion Prevention Technology with CO_2 and N_2 in Goaf*, Safety in Coal Mines, vol. 49, no. 7, pp. 52–61, 2018.

[16] N. I. Akinin, V. M. Raikova, and K. N. Khvostantseva, "Influence of the amine structure on the combustion and explosion of vapor–air mixtures," *Coke and Chemistry*, vol. 59, no. 12, pp. 478–482, 2016.

[17] U. Kadri, R. F. Mudde, R. V. A. Oliemans, M. Bonizzi, and P. Andreussi, "Prediction of the transition from stratified to slug flow or roll-waves in gas–liquid horizontal pipes," *International Journal of Multiphase Flow*, vol. 35, no. 11, pp. 1001–1010, 2009.

[18] X. Zhao, *The Research on the Recurrence of Gas Explosion in Coal Mine*, Changchun University of Science and Technology, Changchun, China, 2006.

[19] J. Li, G. Ma, M. Abdel-Jawad, and H. Hao, "Evaluation of gas explosion overpressures at configurations with irregularly arranged obstacles," *Journal of Performance of Constructed Facilities*, vol. 29, no. 5, article B4014003, 2015.

[20] H. B. Wang and C. J. Yu, "Study on animal injury of gas explosion in pipeline under obstacles conditions," *Journal of North University of China*, vol. 32, no. 6, pp. 727–731, 2011.

[21] B. E. Launder and D. B. Spalding, *Lectures in Mathematical Models of Turbulence*, Academic Press, London, UK, 1972.

[22] R. Taylor and R. Krishna, *Multicomponent Mass Transfer*, Wiley, New York, NY, USA, 1993.

[23] L. Sirovich, "Turbulence and the dynamics of coherent structures part I: coherent structures," *Quarterly of Applied Mathematics.*, vol. 45, no. 3, pp. 561–567, 1987.

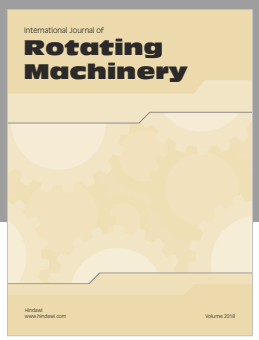

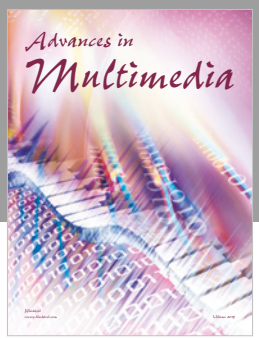

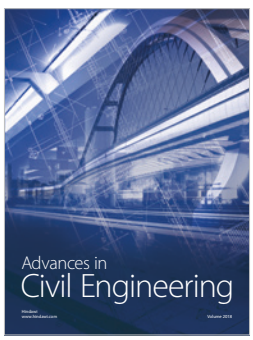

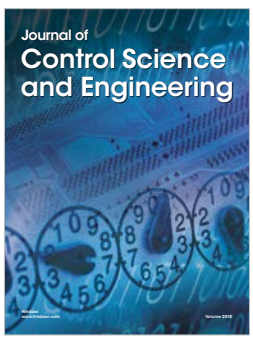

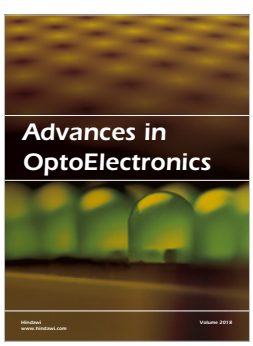

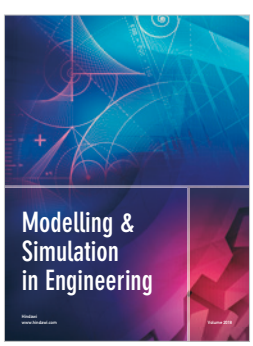

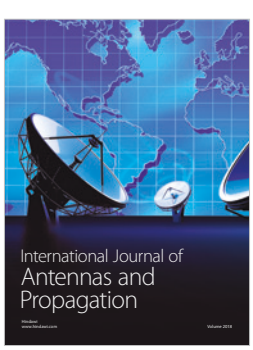

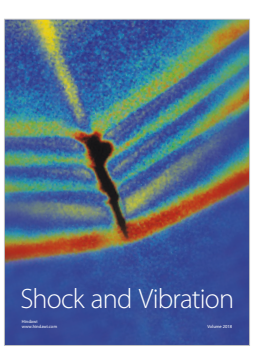

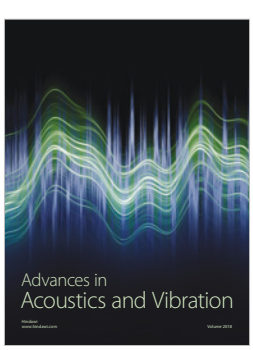

Hindawi

Submit your manuscripts at
www.hindawi.com